

# Quantum phase transitions of 2-d dimerized spin-1/2 Heisenberg models with spatial anisotropy

M.-T. Kao,<sup>1</sup> D.-J. Tan,<sup>1</sup> and F.-J. Jiang<sup>1,\*</sup>

<sup>1</sup>*Department of Physics, National Taiwan Normal University, 88, Sec.4, Ting-Chou Rd., Taipei 116, Taiwan*

Motivated by the unexpected Monte Carlo results as well as the theoretical proposal of a large correction to scaling for the critical theory of the 2-d staggered-dimer spin-1/2 Heisenberg model on the square lattice, we study the phase transitions induced by dimerization of several dimerized quantum Heisenberg models with spatial anisotropy using first principles Monte Carlo method. We focus on investigating the finite-size scaling of the observables  $\rho_{s1}2L$  and  $\rho_{s2}2L$  since such strategy might reveal the subtlety of determining the corresponding critical theory. Here,  $\rho_{si}$  with  $i \in \{1, 2\}$  and  $L$  refer to the spin stiffness in the  $i$  direction and the spatial box size used in the simulations, respectively. Remarkably, while the Monte Carlo data we obtain for all the models considered here, including the herringbone- and ladder-dimer models on the square lattice, seem to be compatible with the recently proposed scenario of an enhanced correction to scaling, our data are in consistence with the established numerical values for the critical exponents in the  $O(3)$  universality class as well. To explain the results presented in this study, a more detailed numerical study, and possibly a better theoretical understanding, for the critical theories of the models investigated here is required.

## I. INTRODUCTION

While being well-studied and understood thoroughly, the dimerized quantum Heisenberg models with spatial anisotropy have triggered theoretical interests again recently [1–12]. For example, the 3-d spatially anisotropic quantum Heisenberg model with a ladder dimerization pattern is used to demonstrate a universal behavior, which is argued to be relevant for understanding the experimental results of the material  $\text{TiCuCl}_3$  [13]. Further, the 2-d dimerized spin-1/2 Heisenberg model with a spatially staggered anisotropy is of particularly interesting because this model seems to establish an unconventional phase transition [14]. Specifically, although it is believed that the phase transition induced by dimerization for this model should be governed by the  $O(3)$  universality class theoretically [15–19], a recent large scale Monte Carlo calculation obtains  $\nu = 0.689(5)$  and  $\beta/\nu = 0.545(5)$ , which are in contradiction to the established  $O(3)$  results  $\nu = 0.7112(5)$  and  $\beta/\nu = 0.519(1)$  in the literature [20]. Here  $\nu$  and  $\beta$  are the critical exponents corresponding to the correlation length and the magnetization, respectively. In order to clarify this issue further, several efforts have been devoted to study the phase transition of this model induced by dimerization. For instance, an unconventional finite-size scaling is proposed in [21]. Further, in [22] it is argued that, due to a cubic term, there is a large correction to scaling for this phase transition which results in the unexpected  $\nu = 0.689(5)$  and  $\beta/\nu = 0.545(5)$  obtained in [14]. Later, a Monte Carlo study indeed provides strong evidence to support this scenario of an enhanced correction to scaling [21]. In addition to the staggered-dimer spin-1/2 Heisenberg model on the square lattice, in [22] it concludes as well that

a similar model on the honeycomb lattice, which is depicted in the bottom panel of figure 1<sup>1</sup>, as well as the herringbone-dimer model on the square lattice (middle panel of figure 1) also belong to the same category of models receiving an enhanced correction. This general picture regarding the correction to scaling for 2-d dimerized quantum Heisenberg models is indeed supported by several related Monte Carlo studies [3, 23–26].

While the Monte Carlo data of the staggered-dimer model on the square lattice provides convincing evidence for the proposal of an enhanced correction to scaling, the most noticeable observation regarding the critical behavior of this model is the good scaling property of the observable  $\rho_{s2}2L$  [21], where again  $\rho_{s2}$  and  $L$  are the spin stiffness in the 2-direction and the spatial box size employed in the simulations, respectively. Inspired by this observation, one naturally would like to examine whether for the staggered-dimer model on the honeycomb lattice and the herringbone-dimer model on the square lattice, a similar good scaling behavior will be observed when considering the same observable  $\rho_{s2}2L$  for these two dimerized models. Although the phase transition induced by dimerization of the staggered-dimer model on the honeycomb lattice has been studied before, a detailed comparison between the scaling behavior of  $\rho_{s1}2L$  and  $\rho_{s2}2L$  as well as the relevant investigation of the exponent  $\beta/\nu$  are not available yet<sup>2</sup>. Further, to examine whether the enhanced correction to scaling, as suggested in [22], does have impact on the determination of the exponents  $\nu$  and  $\beta/\nu$  for the herringbone-dimer model is an interesting topic to explore as well<sup>3</sup>. Hence

<sup>1</sup> We will call this model the staggered-dimer model as well unless confusion arises.

<sup>2</sup> An unpublished work of determining  $\beta/\nu$  is available in [27].

<sup>3</sup> An unpublished work of studying the critical theory for the herringbone-dimer model is available in [27].

\*fjjiang@ntnu.edu.tw

in this study, we have investigated the phase transitions of the herringbone- and ladder-dimer spin-1/2 Heisenberg models on the square lattice, as well as the quantum staggered-dimer model on the honeycomb lattice. In particular, the largest lattice sizes reached here are as twice large as those of the relevant early studies in some cases. The results for the ladder-dimer model are included here for completeness and comparison purpose, since the enhanced correction to scaling should be absent for this model. Remarkably, as we will demonstrate later, indeed  $\rho_{s2}2L$  of the staggered-dimer model on the honeycomb lattice shows a good scaling behavior. Consequently, we are able to obtain a value for  $\nu$ , in agreement with the established  $\nu = 0.7112(5)$  in the  $O(3)$  universality class, by employing the leading scaling ansatz in our finite-size scaling analysis for  $\rho_{s2}2L$ . Interestingly, while the Monte Carlo data we obtain for all the models studied here, including the herringbone- and ladder-dimer models on the square lattice, seem to be compatible with the recently proposed scenario of an enhanced correction to scaling for the phase transitions considered here, our data are also in consistence with the established results of  $\nu = 0.7112(5)$ ,  $\beta/\nu = 0.519(1)$ , and  $\omega \sim 0.78$  ( $\omega$  is the confluent exponent) in the  $O(3)$  universality class. To explain the results presented in this study, a more detailed numerical study, and possibly a better theoretical understanding, for the critical theories of the models investigated here is required.

This paper is organized as follows. First, after an introduction, the spatially anisotropic quantum Heisenberg models and the relevant observables studied in this work are briefly described, after which we present our numerical results. In particular, the results obtained from the finite-size scaling analysis are discussed in detail. A final section then concludes our study.

## II. MICROSCOPIC MODEL AND CORRESPONDING OBSERVABLES

The Heisenberg models considered in this study are defined by the Hamilton operator

$$H = \sum_{\langle xy \rangle} J \vec{S}_x \cdot \vec{S}_y + \sum_{\langle x'y' \rangle} J' \vec{S}_{x'} \cdot \vec{S}_{y'}, \quad (1)$$

where  $J$  and  $J'$  are antiferromagnetic exchange couplings connecting nearest neighbor spins  $\langle xy \rangle$  and  $\langle x'y' \rangle$ , respectively. Figure 1 illustrates the models which are described by Eq. (1) and are investigated in great detail here. To study the critical behavior of these models near the transition driven by the anisotropy, in particular, to determine the critical points as well as the critical exponent  $\nu$ , the spin stiffnesses in the 1- and 2-directions which are defined by

$$\rho_{si} = \frac{1}{\beta L^2} \langle W_i^2 \rangle, \quad (2)$$

are measured in our simulations. Here  $\beta$  is the inverse temperature and  $L$  again refers to the spatial box size.

Further  $\langle W_i^2 \rangle$  with  $i \in \{1, 2\}$  is the winding number squared in the  $i$  direction. In addition, the second Binder ratio  $Q_2$ , which is defined by

$$Q_2 = \frac{\langle (m_s^z)^2 \rangle^2}{\langle (m_s^z)^4 \rangle}, \quad (3)$$

is also measured in our simulations as well. Here  $m_s^z$  is the  $z$  component of the staggered magnetization  $\vec{m}_s = \frac{1}{L^2} \sum_x (-1)^{x_1+x_2} \vec{S}_x$ . By carefully investigating the spatial volume and the  $J'/J$  dependence of  $\rho_{si}L$  as well as  $Q_2$ , one can determine the critical points and the critical exponent  $\nu$  with high precision. Finally the exponent  $\beta/\nu$  is determined by studying the scaling behavior of the observables  $\langle |m_s^z| \rangle$  and  $\langle (m_s^z)^2 \rangle$ , which are measured in this study as well, at the corresponding critical points.

## III. DETERMINATION OF THE CRITICAL POINTS AND THE CRITICAL EXPONENT $\nu$

To study the quantum phase transitions of our central interest, we have carried out large scale Monte Carlo simulations using a loop algorithm [28–32]. Further, to calculate the relevant critical exponent  $\nu$  and to determine the location of the critical points in the parameter space  $J'/J$  for the models described by figure 1, we have employed the technique of finite-size scaling for certain observables. For example, if a transition is second order, then near the transition the observable  $\rho_{si}2L$  for  $i \in \{1, 2\}$  and  $Q_2$  should be described well by the following finite-size scaling ansatz [33–37]

$$\begin{aligned} \mathcal{O}_L(t) &= g_{\mathcal{O}}(tL^{1/\nu}, L^z/\beta, r) + L^{-\omega} g_{\mathcal{O}\omega}(tL^{1/\nu}, L^z/\beta, r) \\ &= g_{\mathcal{O}}(tL^{1/\nu}, L^z/\beta, r) \times \\ &\quad \left( 1 + L^{-\omega} g'_{\mathcal{O}\omega}(tL^{1/\nu}, L^z/\beta, r) \right) \end{aligned} \quad (4)$$

where  $\mathcal{O}_L$  stands for  $Q_2$  and  $\rho_{si}L$  with  $i \in \{1, 2\}$ ,  $L$  is the lattice size in the 1-direction,  $t = (j_c - j)/j_c$  with  $j = (J'/J)$ ,  $\nu$  is the critical exponent corresponding to the correlation length  $\xi$ ,  $\omega$  is the confluent correction exponent,  $z$  is the dynamical critical exponent which is 1 for the phase transitions considered here, and  $r$  is the ratio of the lattice size in the 1- and 2-direction. Further,  $g_{\mathcal{O}}$ ,  $g_{\mathcal{O}\omega}$ , and  $g'_{\mathcal{O}\omega}$  appearing above are smooth functions of the variables  $tL^{1/\nu}$ ,  $L/\beta$ , and  $r$ . In practice one would carry out the analysis close to the critical point so that  $g'_{\mathcal{O}\omega}$  in Eq. (4) can be approximated by a constant. Specifically, the following ansatz

$$\mathcal{O}_L(t) = (1 + bL^{-\omega})g_{\mathcal{O}}(tL^{1/\nu}, L^z/\beta, r), \quad (5)$$

where  $b$  is some constant, is frequently used when applying the finite-size scaling technique. While Eq. (5) is only valid for large box sizes and close to the critical point, to present the main results of this study we find it is sufficient to employ Eq. (5) for the data analysis. Notice that for square lattice or rectangular-shape lattice with

a fixed  $r$ , one will intuitively neglect the effect of  $r$  in Eq. (5). Hence, we will apply Eq. (5) with a constant  $r$  to the relevant observables for obtaining  $(J'/J)_c$  and  $\nu$ . Notice from Eq. (5), one concludes that the curves for  $\mathcal{O}_L$  corresponding to different  $L$ , as functions of  $J'/J$ , should intersect at the critical point  $(J'/J)_c$  for large  $L$ . Without loss of generality, we have fixed  $J = 1$  in our simulations and have varied  $J'$ . Additionally, the box size used in the simulations ranges from  $L = 24$  to  $L = 136$  (Strictly speaking,  $L = \sqrt{N}$  for the staggered-dimer model on the honeycomb lattice. Here  $N$  is the number of spins used in the simulations). To reach a lattice size as large as possible, we use  $\beta J = 2L$  for each  $L$  in our simulations. Consequently, the temperature dependence in Eq. (5) drops out. First of all, let us focus on our results for the staggered-dimer spin-1/2 Heisenberg model on the honeycomb lattice.

### A. Results for the staggered-dimer spin-1/2 Heisenberg model on the honeycomb lattice

Figure 2 shows the Monte Carlo data of  $\rho_{s1}2L$ ,  $\rho_{s2}2L$ , and  $Q_2$  with  $24 \leq L \leq 96$  as functions of  $J'/J$  for the staggered-dimer spin-1/2 Heisenberg model on the honeycomb lattice. The figure clearly indicates that the phase transition is most likely second order since for all the observables  $\rho_{s1}2L$ ,  $\rho_{s2}2L$ , and  $Q_2$ , the curves of different  $L$  tend to intersect near a particular point in the parameter space  $J'/J$ . A surprising observation from figure 2 is that, while  $\rho_{s1}2L$  receives a sizable correction to its scaling (which has already been shown in [26]), the observable  $\rho_{s2}2L$  shows a good scaling behavior. Specifically, the correction to scaling for  $\rho_{s2}2L$  is negligible for  $L \geq 32$ . These findings are similar to the scenario regarding the correction to scaling for the same observables, namely  $\rho_{s1}2L$  and  $\rho_{s2}2L$ , of the staggered-dimer model on the square lattice [21]. Indeed, from  $\rho_{s2}2L$  with  $L \geq 32$ , we are able to reach a value for  $\nu$  compatible with the expected  $\nu = 0.7112(5)$  using the leading finite-size scaling ansatz in Eq. (5) (letting  $b = 0$  in Eq. (5)). For example, the  $\nu$  obtained from applying a second order Taylor expansion in  $tL^{1/\nu}$  of Eq. (5) with  $b = 0$  to the observable  $\rho_{s2}2L$  with  $40 \leq L \leq 96$  is given by  $\nu = 0.7167(40)$ , which is in nice agreement with its theoretical expectation in the literature. To reach a value for  $\nu$  consistent with  $\nu = 0.7112(5)$  using the leading finite-size scaling ansatz and the observable  $\rho_{s1}2L$ , one has to use data with fairly large  $L$  as indicated in [26]. Indeed a similar conclusion is reached here. Interestingly, with the observable  $\rho_{s1}2L$ , while we either arrive at values of  $\nu$  statistically different from  $\nu = 0.7112(5)$  or cannot reach good results when  $b$  and  $\omega$  in Eq. (5) are included as fitting parameters, compatible results of  $\nu$  with  $\nu = 0.7112(5)$  can be obtained from the fits with the assumption that  $\omega \leq 0.5$  is used as a criterion for the fits. For instance, using  $\rho_{s1}2L$  with  $40 \leq L \leq 96$ , the values of  $\nu$  and  $\omega$  determined from the fits by employ-

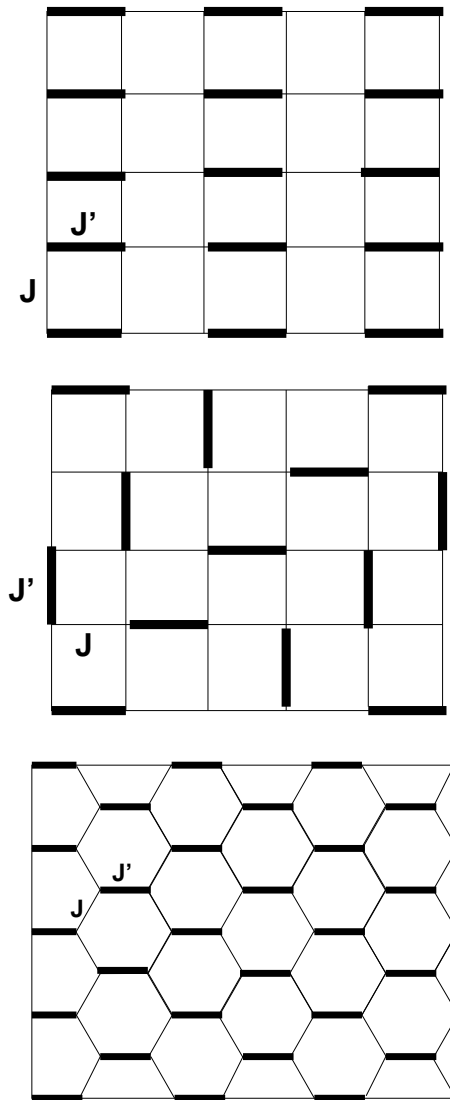


FIG. 1: The dimerized quantum Heisenberg models with spatial anisotropy considered in this study.

ing the criterion of  $\omega \leq 0.5$  are given by  $\nu = 0.7054(45)$  and  $\omega = 0.42(8)$ , respectively. Notice  $\omega \sim 0.42$  is smaller than the expected  $\omega \sim 0.78$  in the  $O(3)$  universality class. One might conclude that our results are consistent with the scenario outlined in [22] that the correction to scaling for this model is enhanced due to a cubic irrelevant term. Finally, from  $Q_2$  with  $32 \leq L \leq 96$ , a fit using Taylor expansion to second order in  $tL^{1/\nu}$  as well as letting  $b = 0$  in Eq. (5) leads to  $\nu = 0.7102(56)$  and  $(J'/J)_c = 1.73560(4)$ , both of which agree quantitatively with the known results in the literature. Interestingly, the obtained coefficients for  $(tL^{1/\nu})^2$  in the fits associated with  $Q_2$  are very small. Hence, we can even reach a value for  $\nu$  in agreement with  $\nu = 0.7112(5)$  using a first order Taylor expansion in  $tL^{1/\nu}$  of Eq. (5) to fit the data points of  $Q_2$  (the last 2 rows in table 1). The values of  $\nu$

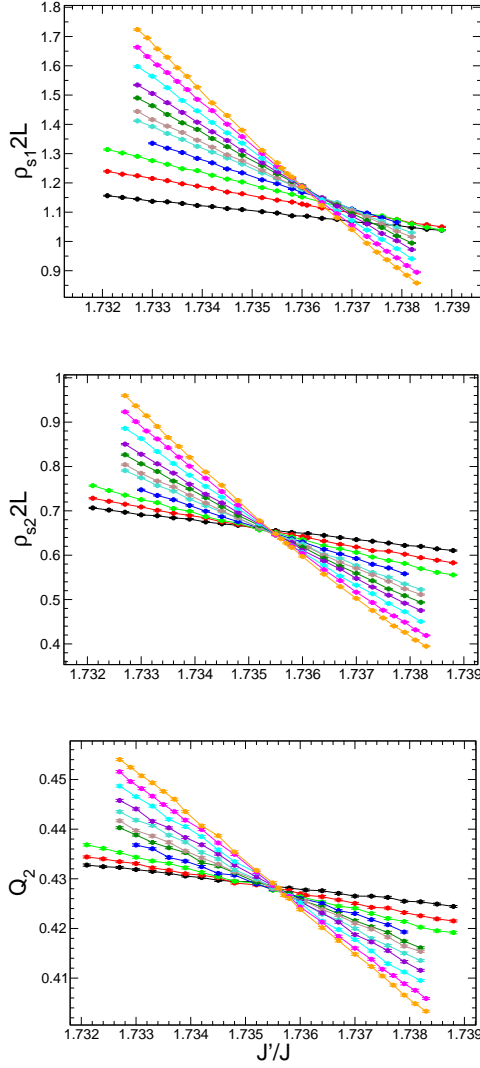


FIG. 2: Monte Carlo data of  $\rho_{s1}2L$ ,  $\rho_{s2}2L$ , and  $Q_2$  with  $24 \leq L \leq 96$  for the staggered-dimer spin-1/2 Heisenberg model on the honeycomb lattice.

and  $(J'/J)_c$  obtained from the fits mentioned above are listed in table 1. Notice that the uncertainties of  $(J'/J)_c$  and  $\nu$  shown in table 1, as well as in tables 2, 3, 4, and 5 in the following sections, are determined by a conservative estimate based on the standard deviations obtained from the bootstrap resampling method employed for the fits.

### B. Results for the herringbone-dimer spin-1/2 Heisenberg model on the square lattice

After having calculated  $(J'/J)_c$  and  $\nu$  for the phase transition induced by dimerization of the staggered-dimer spin-1/2 Heisenberg model on the honeycomb lattice, we turn to investigating the corresponding critical theory of the herringbone-dimer model on the square lat-

observable	$L$	$\nu$	$(J'/J)_c$	$\chi^2/\text{DOF}$
$\rho_{s1}2L$	$40 \leq L \leq 96$	0.7054(45)	1.7355(2)	1.2
$\rho_{s1}2L$	$48 \leq L \leq 96$	0.7096(55)	1.7355(3)	1.2
$\rho_{s2}2L$	$32 \leq L \leq 96$	0.7156(40)	1.73545(3)	1.9
$\rho_{s2}2L$	$40 \leq L \leq 96$	0.7167(40)	1.73548(3)	1.4
$\rho_{s2}2L$	$48 \leq L \leq 96$	0.7055(42)*	1.73550(3)*	0.9
$\rho_{s2}2L$	$56 \leq L \leq 96$	0.7082(45)*	1.73551(3)*	0.9
$Q_2$	$32 \leq L \leq 96$	0.7102(56)	1.73560(4)	1.4
$Q_2$	$40 \leq L \leq 96$	0.712(6)	1.73570(5)	1.3
$Q_2$	$32 \leq L \leq 96$	0.7107(56) $^\diamond$	1.73564(3) $^\diamond$	1.4
$Q_2$	$40 \leq L \leq 96$	0.712(6) $^\diamond$	1.73566(4) $^\diamond$	1.4

TABLE I: The numerical values of  $\nu$  and  $(J'/J)_c$  calculated from  $\rho_{s1}2L$ ,  $\rho_{s2}2L$ , and  $Q_2$  for the staggered-dimer model on the honeycomb lattice. All results are obtained by using a second order Taylor expansion in  $tL^{1/\nu}$  of Eq. (5) except those with a star (diamond) which are determined by a third order (first order) Taylor expansion. The confluent correction is included in the fit explicitly only for  $\rho_{s1}2L$  and is assumed to satisfy the condition  $\omega \leq 0.5$ .

observable	$L$	$\nu$	$(J'/J)_c$	$\chi^2/\text{DOF}$
$\rho_s L$	$24 \leq L \leq 136$	0.705(2)	2.49804(8)	1.4
$\rho_s L$	$24 \leq L \leq 96$	0.706(3)	2.4980(2)	1.4
$\rho_s L$	$24 \leq L \leq 72$	0.702(5)	2.4980(5)	1.1
$\rho_s L$	$32 \leq L \leq 136$	0.706(2)	2.49805(10)	1.4
$\rho_s L$	$32 \leq L \leq 96$	0.707(3)	2.4980(3)	1.4
$\rho_s L$	$24 \leq L \leq 72$	0.700(4)*	2.49813(10)*	1.1
$\rho_s L$	$32 \leq L \leq 136$	0.706(2)*	2.49806(3)*	1.5
$\rho_s L$	$32 \leq L \leq 96$	0.707(3)*	2.49806(7)*	1.4
$Q_2$	$24 \leq L \leq 136$	0.714(4)	2.49800(7)	0.9
$Q_2$	$32 \leq L \leq 136$	0.715(6)	2.4980(2)	1.1
$Q_2$	$24 \leq L \leq 136$	0.710(4)*	2.49820(6)*	1.1
$Q_2$	$24 \leq L \leq 96$	0.716(5)*	2.4983(1)*	1.1
$\rho_s L$	$24 \leq L \leq 136$	0.701(2)	2.49803(7)	1.2
$\rho_s L$	$32 \leq L \leq 136$	0.702(3)	2.4980(1)	1.2
$Q_2$	$24 \leq L \leq 136$	0.707(4)	2.49800(15)	0.8
$Q_2$	$32 \leq L \leq 136$	0.7075(45)	2.4980(2)	0.9
$Q_2$	$32 \leq L \leq 136$	0.7056(40)*	2.49810(6)*	0.9
$Q_2$	$40 \leq L \leq 136$	0.7065(40)*	2.49810(7)*	0.8

TABLE II: The numerical values of  $\nu$  and  $(J'/J)_c$  calculated from  $\rho_s L$  and  $Q_2$  for the herringbone-dimer model on the square lattice. While the results presented in the first twelve rows are obtained by using a second order Taylor expansion in  $tL^{1/\nu}$  of Eq. (5), those listed in the last six rows are determined with a third order Taylor expansion. Further, all results are calculated with the  $\omega$  and  $b$  in Eq. (5) left as fitting parameters except those with a star which are determined through fits with a fixed  $\omega = 0.78$ .



observable	$L$	$\nu$	$\omega$	$\chi^2/\text{DOF}$
$\rho_s L$	$24 \leq L \leq 136$	0.708(5)	0.53(3)	1.6
$\rho_s L$	$32 \leq L \leq 136$	0.710(5)	0.57(5)	1.7
$\rho_s L$	$40 \leq L \leq 136$	0.711(6)	0.63(8)	1.7
$\rho_s L$	$24 \leq L \leq 96$	0.706(8)	0.48(5)	1.6
$\rho_s L$	$24 \leq L \leq 136$	0.711(7)*	N/A	2.0
$\rho_s L$	$32 \leq L \leq 136$	0.711(6)*	N/A	1.8
$Q_2$	$24 \leq L \leq 136$	0.710(5)	2.2(1)	0.9
$Q_2$	$32 \leq L \leq 136$	0.710(5)	2.42(25)	0.9
$Q_2$	$24 \leq L \leq 96$	0.712(7)	2.10(13)	1.0
$Q_2$	$24 \leq L \leq 136$	0.714(9)*	N/A	1.8
$Q_2$	$32 \leq L \leq 136$	0.712(7)*	N/A	1.2

TABLE III: The numerical values of  $\nu$  and  $(J'/J)_c$  calculated from  $\rho_s L$  and  $Q_2$  for the herringbone-dimer model on the square lattice. All results are obtained by using a first order Taylor expansion in  $tL^{1/\nu}$  of Eq. (5) with  $\omega$  and  $b$  left as fitting parameters except those with a star which are determined through fits with a fixed  $\omega = 0.78$ .

tice. Since for this model one has  $\rho_{s1} = \rho_{s2}$ , the relevant observables used in our finite-size scaling analysis are  $\rho_s L$ , which is the average of  $\rho_{s1} L$  and  $\rho_{s2} L$ , and the second Binder ratio  $Q_2$  (figure 3). To calculate  $\nu$ , we first carry out several analysis by employing the second order Taylor expansion in  $tL^{1/\nu}$  of Eq. (5), with the subleading correction included explicitly, to fit our Monte Carlo data of  $\rho_s L$  with variant range of  $L$ . Remarkably, a numerical value of  $\nu$  compatible with  $\nu = 0.7112(5)$  can be obtained if the smallest and largest box sizes used in the fits are larger than 24 and 96, respectively. The results of  $(J'/J)_c$  and  $\nu$  calculated from these fits are listed as the first 5 rows in table 2. Further, the values of  $\omega$  determined from these fits ranges from 0.58 to 0.79 with an average of 0.66. Notice  $\omega \sim 0.66$  we obtain is slightly below the expected  $\omega \sim 0.78$  in the  $O(3)$  universality class, hence is consistent with the scenario suggested in [22]. However, these results for  $\omega$  should only be considered as effective ones. Similarly, a fit using  $Q_2$  with  $24 \leq L \leq 136$  as well as a second order Taylor expansion in  $tL^{1/\nu}$  of Eq. (5), with the confluent correction left as fitting parameters for the fit, leads to  $(J'/J)_c = 2.49800(7)$  and  $\nu = 0.714(4)$ . Notice the determined  $\nu = 0.714(4)$  is consistent with  $\nu = 0.7112(5)$ . Further, the confluent exponent  $\omega$  from the fit is given by  $\omega = 2.0(2)$ . Finally, while using other range of  $L$  for  $Q_2$  we can arrive at values of  $\nu$  agreeing with  $\nu = 0.7112(5)$ , the  $\omega$  calculated from these additional fits are poor determined. Notice that a second order Taylor expansion in  $tL^{1/\nu}$  of Eq. (5) with the subleading correction included for the fit contains seven fitting parameters, which is at the border of reasonable amount of the unknown coefficients for a fit. Still, one would like to understand whether a consistent  $\nu$  with  $\nu = 0.7112(5)$  can be obtained from the fits with fewer fitting parameters. Interestingly, using  $(J'/J)_c = 2.4980$ ,

the data points very close to the critical point, as well as a first order Taylor expansion in  $tL^{1/\nu}$  of Eq. (5) with the confluent correction included explicitly (which has five unknown coefficients), the values of  $\nu$  determined from these new fits for both  $\rho_s L$  and  $Q_2$  are compatible with  $\nu = 0.7112(5)$  (table 3 and top panel of figure 4). Therefore we conclude that, our data points of  $\rho_s L$  and  $Q_2$  for the herringbone-dimer model on the square lattice indeed can be described nicely with the expected  $\nu = 0.7112(5)$  in the  $O(3)$  universality class. Notice that the values of  $\omega$  calculated from the additional fits (first order Taylor expansion of Eq. (5)) related to  $\rho_s L$  has an average of 0.55, hence again is in agreement with the scenario of a large correction to scaling for this phase transition induced by spatial anisotropy.

Interestingly, while the results we obtain so far are in consistence with the scenario of a large correction to scaling as suggested in [22], the numerical values of  $\nu$  determined from the fits with a fixed  $\omega = 0.78$  are also compatible with  $\nu = 0.7112(5)$  for both  $\rho_s L$  and  $Q$  (table 2 and table 3). For instance, a fit using a fixed  $\omega = 0.78$  to the observable  $\rho_s L$  with  $32 \leq L \leq 96$  leads to  $\nu = 0.707(3)$ , which is in nice agreement with the expected result of  $\nu = 0.7112(5)$ . Further, we are also able to arrive at values of  $\nu$  agreeing with  $\nu = 0.7112(5)$  using the first order Taylor expansion in  $tL^{1/\nu}$  of Eq. (5) with a fixed  $\omega = 0.78$  for the fits (table 3). These additional fits contains only four unknown coefficients. Hence, both the strategies of fixing  $\omega$  to be 0.78 or letting it be a fitting parameter lead to results of  $\nu$  consistent with  $\nu = 0.7112(5)$ . Notice in our earlier calculations using a second order Taylor expansion of the full ansatz Eq. (5), although the mean average of  $\omega$ , determined from the fits with both the  $b$  and  $\omega$  in Eq. (5) left as fitting parameters, is smaller than the expected 0.78 in most of the cases, the uncertainties for  $\omega$  from these fits are large. Hence, for a spread range  $(a_1, a_2)$  of  $\omega$  (i.e.  $\omega \in (a_1, a_2)$ ), consistent  $\nu$  with  $\nu = 0.7112(5)$  is obtained from the fits using the chosen  $\omega$  in  $(a_1, a_2)$ . Therefore, it might be premature to conclude that the confluent exponent  $\omega$  for this phase transition is indeed smaller than 0.78 just from what we have obtained so far. In addition, since the values of  $\omega$  obtained from the fits might be contaminated by higher order terms, a more sophisticated determination of  $\omega$  should be performed.

### C. Results for the ladder-dimer spin-1/2 Heisenberg model on the square lattice

The final dimer model considered in this study is the 2-d quantum Heisenberg model on the square lattice with a ladder spatial anisotropy, which has been studied extensively in the literature. Here for completeness, we have re-investigated the phase transition induced by dimerization of this model. Intuitively, due to their similarity, one might expect that the good scaling behavior of the observable  $\rho_{s2} 2L$ , found for the staggered-dimer model

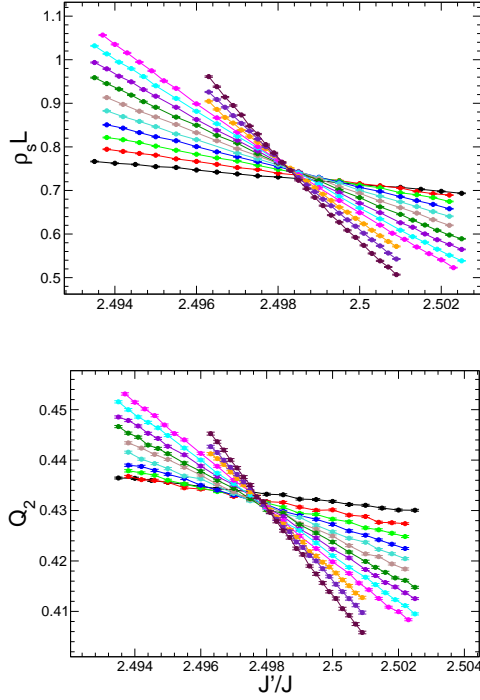


FIG. 3: Monte Carlo data of  $\rho_s L$  and  $Q_2$  with  $24 \leq L \leq 136$  for the herringbone-dimer spin-1/2 Heisenberg model on the square lattice.

on both the square and honeycomb lattices, will emerge again for the ladder-dimer model. Interestingly, the effects of the correction to scaling for  $\rho_{s1}2L$  and  $\rho_{s2}2L$  of this model are about the same qualitatively (figure 4). This indicates the fundamental difference regarding the correction to scaling between the staggered- and ladder-dimer models as suggested in [22]. Similar to the analysis performed for obtaining  $\nu$  and  $(J'/J)_c$  for the herringbone-dimer model, a second order Taylor expansion in  $tL^{1/\nu}$  of Eq. (5), with the subleading correction included explicitly, is employed to fit the Monte Carlo data of  $\rho_{s1}2L$  with variant range of  $L$ . The obtained  $(J'/J)_c$  and  $\nu$  are in table 4. Interestingly, table 4 implies that a result for  $\nu$  compatible with  $\nu = 0.7112(5)$  can be obtained as well if the smallest and largest box sizes used in the fits are larger than 24 and 96, respectively. Further, although with considerable large uncertainties, most the values of  $\omega$  determined from these fits are smaller than 0.78 and are compatible in magnitude with those determined from the herringbone-dimer model. In addition, using  $(J'/J)_c = 1.9095$ , the data points very close to the critical point, as well as a first order Taylor expansion in  $tL^{1/\nu}$  of the full ansatz Eq. (5), the values of  $\nu$  determined from these new fits for  $\rho_{s1}2L$  are compatible with  $\nu = 0.7112(5)$  (table 5 and bottom panel of figure 4). Therefore we conclude that, our data points of  $\rho_{s1}2L$  for the ladder-dimer model on the square lattice indeed can be described nicely with the expected  $\nu = 0.7112(5)$  in the  $O(3)$  universality class. Finally, similar to the results

observable	$L$	$\nu$	$(J'/J)_c$	$\chi^2/\text{DOF}$
$\rho_{s1}2L$	$24 \leq L \leq 136$	0.707(2)	1.90955(9)	1.1
$\rho_{s1}2L$	$24 \leq L \leq 96$	0.705(3)	1.9096(2)	1.2
$\rho_{s1}2L$	$24 \leq L \leq 72$	0.696(5)	1.9095(6)	1.1
$\rho_{s1}2L$	$32 \leq L \leq 136$	0.708(2)	1.90956(12)	1.1
$\rho_{s1}2L$	$32 \leq L \leq 96$	0.706(3)	1.9097(2)	1.1
$\rho_{s1}2L$	$24 \leq L \leq 136$	0.706(2)*	1.90960(3)*	1.2
$\rho_{s1}2L$	$32 \leq L \leq 72$	0.698(5)*	1.90956(16)*	1.1
$\rho_{s1}2L$	$32 \leq L \leq 96$	0.707(3)*	1.90961(7)*	1.2
$\rho_{s1}2L$	$24 \leq L \leq 136$	0.704(3)	1.9095(1)	1.1
$\rho_{s1}2L$	$32 \leq L \leq 136$	0.705(3)	1.90956(13)	1.1

TABLE IV: The numerical values of  $\nu$  and  $(J'/J)_c$  calculated from  $\rho_{s1}2L$  for the ladder-dimer model on the square lattice. While the results presented in the first eight rows are obtained by using a second order Taylor expansion in  $tL^{1/\nu}$  of Eq. (5), those listed in the last two rows are determined with a third order Taylor expansion. Further, all results are calculated with the  $\omega$  and  $b$  in Eq. (5) left as fitting parameters except those with a star which are determined through fits with a fixed  $\omega = 0.78$ .

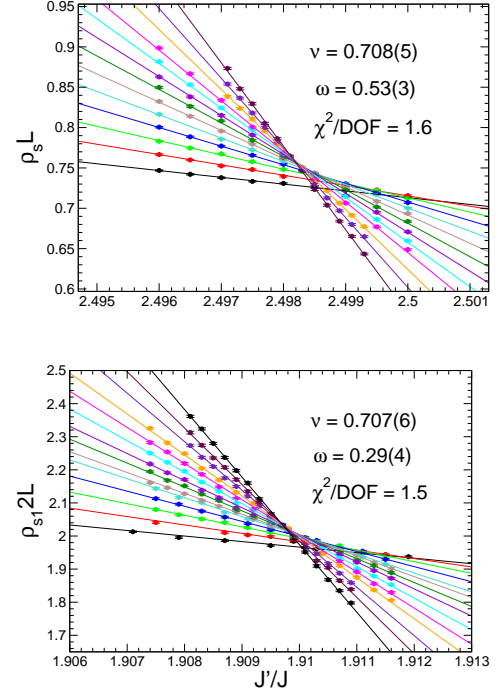


FIG. 4: Fits of  $\rho_s L$  ( $24 \leq L \leq 136$ ) of the herringbone-dimer model (top panel) and  $\rho_{s1}2L$  ( $24 \leq L \leq 136$ ) of the ladder-dimer model (bottom panel) to the first order Taylor expansion in  $tL^{1/\nu}$  of the full ansatz Eq. (5). While the circles are the numerical Monte Carlo data from the simulations, the solid curves are obtained by using the results from the fits.

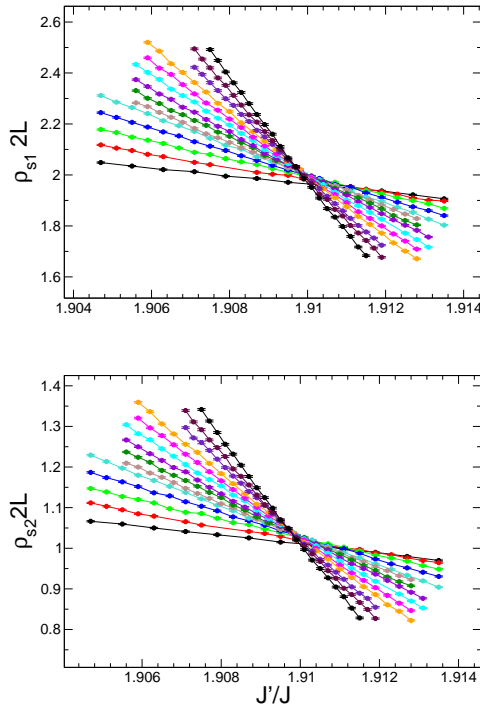


FIG. 5: Monte Carlo data of  $\rho_{s1}2L$  and  $\rho_{s2}2L$  with  $24 \leq L \leq 136$  for the ladder-dimer spin-1/2 Heisenberg model on the square lattice.

observable	$L$	$\nu$	$\omega$	$\chi^2/\text{DOF}$
$\rho_{s1}2L$	$24 \leq L \leq 136$	0.707(6)	0.29(4)	1.5
$\rho_{s1}2L$	$32 \leq L \leq 136$	0.709(6)	0.26(6)	1.5
$\rho_{s1}2L$	$24 \leq L \leq 96$	0.703(8)	0.28(6)	1.5

TABLE V: The numerical values of  $\nu$  and  $(J'/J)_c$  calculated from  $\rho_{s1}2L$  for the ladder-dimer model on the square lattice. All results are obtained by using a first order Taylor expansion in  $tL^{1/\nu}$  of the full ansatz Eq. (5).

for the herringbone-dimer model, with a fixed  $\omega = 0.78$ , the values of  $\nu$  calculated from our finite-size scaling analysis are compatible with  $\nu = 0.7112(5)$  as well (table 4).

#### IV. DETERMINATION OF THE EXPONENT $\beta/\nu$

After having calculated the critical exponent  $\nu$  from the relevant observables for the models described by figure 1, we turn to the determination of the exponent  $\beta/\nu$ . To calculate  $\beta/\nu$ , the scaling behavior of the observables  $\langle|m_s^z|\rangle$  and  $\langle(m_s^z)^2\rangle$  are studied. Specifically, at critical points and for large  $L$ , the observable  $\langle|m_s^z|^k\rangle$  should scale

as

$$\langle|m_s^z|^k\rangle = (a_k + b_k L^{-\omega}) L^{-k\beta/\nu}, \quad (6)$$

where  $a_k, b_k$  are some constants for  $k = 1$  and each even positive integer  $k$ . Since precise knowledge of the critical points is essential in determining the exponent  $\beta/\nu$ , we use the values of  $(J/J')_c$  obtained in previous sections when calculating the critical exponent  $\nu$ . Interestingly, as shown in tables 1, 2, and 4, small statistical deviation between some of the determined critical points of the same model is found. We attribute such small discrepancy to the presence of higher order subleading corrections which are not taken into account in our analysis, as well as the fact that the bootstrap resampling method used in calculating  $(J/J')_c$  and  $\nu$  might occasionally leads to underestimated errors. While small deviation is observed, the accuracy of  $(J/J')_c$  presented in tables 1, 2, and 4, is sufficient for determining  $\beta/\nu$  by investigating the scaling behavior of  $\langle|m_s^z|\rangle$  and  $\langle(m_s^z)^2\rangle$ , at the corresponding critical points. Hence, the values of  $(J/J')_c$  for the herringbone- and ladder-dimer models on the square lattice, as well as the staggered-dimer model on the honeycomb lattice are taken to be 2.4980, 1.9095, and 1.7355, respectively. Further, we have carried out additional simulations at these critical points so that the largest lattice size we reach for both the herringbone- and staggered-dimer models is  $L = 184$ . First of all, let us focus on the results of  $\beta/\nu$  obtained from  $\langle|m_s^z|\rangle$ . Interestingly, with the expected leading scaling behavior, only from the ladder-dimer model we are able to reach a value of  $\beta/\nu$  which is in agreement with the established result  $\beta/\nu = 0.519(1)$  in the literature. For example, while a fit using the leading scaling expectation and the observable  $\langle|m_s^z|\rangle$  with  $L \geq 72$  of the ladder-dimer model results in  $\beta/\nu = 0.517(2)$  (top panel of figure 6), the corresponding numerical value of  $\beta/\nu$  determined from the same observable, with a similar range of  $L$ , is given by  $\beta/\nu = 0.527(3)$  ( $\beta/\nu = 0.531(3)$ ) for the herringbone-dimer model (staggered-dimer model on the honeycomb lattice). Further, using  $L \geq 128$  ( $L \geq 120$ ), the value of  $\beta/\nu$  obtained from a fit without the confluent correction for the herringbone-dimer model (staggered-dimer model on the honeycomb lattice) is given by  $\beta/\nu = 0.522(5)$  ( $\beta/\nu = 0.526(3)$ ). At this stage, one might conclude that the correction to scaling for the staggered- and herringbone-dimer models are indeed enhanced as proposed in [22]. In particular, the value of  $\omega$  determined from the related fits should be smaller than the expected  $O(3)$  result  $\omega \sim 0.78$ . Surprisingly, for both the herringbone-dimer model on the square lattice and the staggered-dimer model on the honeycomb lattice, using the data of  $\langle|m_s^z|\rangle$  with  $16 \leq L \leq 184$ , a fit including the subleading correction and a fixed  $\omega = 0.78$  leads to values of  $\beta/\nu$  compatible with  $\beta/\nu = 0.519(1)$  (middle and bottom panels of figure 6). Further, if  $\omega$  is left as a fitting parameter, although consistent  $\beta/\nu$  with  $\beta/\nu = 0.519(1)$  are obtained from the fits associated with the herringbone-dimer model, the uncertainties

for  $\beta/\nu$  and  $\omega$  are increased significantly. For example, the  $\beta/\nu$  and  $\omega$  determined from a fit using  $\langle |m_s^z| \rangle$  with  $16 \leq L \leq 184$  of the herringbone-dimer model are given by  $\beta/\nu = 0.521(9)$  and  $0.86(50)$ , respectively. Finally, a fit to the observable  $\langle |m_s^z| \rangle$  of the ladder-dimer model with a fixed  $\omega = 0.78$  leads to  $\beta/\nu = 0.516(3)$ , which is consistent with  $\beta/\nu = 0.519(1)$  as well. Interestingly, a value of  $\beta/\nu$  slightly below  $\beta/\nu = 0.519(1)$  is reached when the leading scaling prediction is employed to fit all available data of  $\langle |m_s^z| \rangle$  of the ladder-dimer model. This in turn implies that the coefficient  $b_1$  in Eq. (6) for the ladder-dimer model is small in magnitude. Indeed, the magnitude of  $b_1$  obtained from applying the full ansatz Eq. (6) with a fixed  $\omega = 0.78$  to  $\langle |m_s^z| \rangle$  of the ladder-dimer model is of order  $10^{-2}$  (The uncertainty for  $b_1$  is comparable to  $b_1$  in magnitude as well). Finally, we have also carried out an additional analysis with different fixed values of  $\omega$  in the fits. The obtained  $\beta/\nu$  for these additional fits are shown in table 5. From table 5 one concludes that the values of  $\omega$  that would lead to consistent  $\beta/\nu$  with  $\beta/\nu = 0.519(1)$  for both the herringbone- and staggered-dimer models ranges from 0.7 to 0.9, which matches reasonable well with the expected value 0.78. All the results we have reached so far imply that, our data points of  $\langle |m_s^z| \rangle$  for all the three dimerized models depicted in figure 1 are compatible with the established value of  $\omega \sim 0.78$  in the  $O(3)$  universality class.

After having demonstrated that our Monte Carlo data of  $\langle |m_s^z| \rangle$ , for all the three dimerized models investigated here, are compatible with the established results of  $\beta/\nu = 0.519(1)$  and  $\omega = 0.78$  in the  $O(3)$  universality class, a similar scenario is reached when considering the observable  $\langle (m_s^z)^2 \rangle$ . For example, using the leading scaling prediction, only from the ladder-dimer model we can reach a value for  $\beta/\nu$  compatible with  $\beta/\nu = 0.519(1)$  (top panel of figure 7). Further, with a fixed  $\omega = 0.78$ , the fits for the herringbone-dimer model on the square lattice and the staggered-dimer model on the honeycomb lattice result in  $\beta/\nu = 0.5202(15)$  and  $\beta/\nu = 0.518(2)$ , respectively (middle and bottom panels of figure 7). The results of  $\beta/\nu = 0.5202(15)$  and  $\beta/\nu = 0.518(2)$  we just obtain are in quantitative agreement with the expected  $\beta/\nu = 0.519(1)$ . Further, an analysis for  $\langle (m_s^z)^2 \rangle$ , with variant fixed values of  $\omega$  in the fits, leads to a similar conclusion like that of  $\langle |m_s^z| \rangle$ . Specifically, from  $\langle (m_s^z)^2 \rangle$ , the values of  $\omega$  that would lead to consistent  $\beta/\nu$  with  $\beta/\nu = 0.519(1)$  for both the herringbone- and staggered-dimer models ranges from 0.7 to 0.9 as well (table 6).

Tables 4, 5, and 6 summarizes our calculations on determining  $\beta/\nu$  for the phase transitions induced by dimerization for all the three models shown in figure 1.

## V. DISCUSSION AND CONCLUSION

In this study, we investigate the phase transitions induced by dimerization for the herringbone- and ladder-dimer spin-1/2 Heisenberg model on the square lattice,

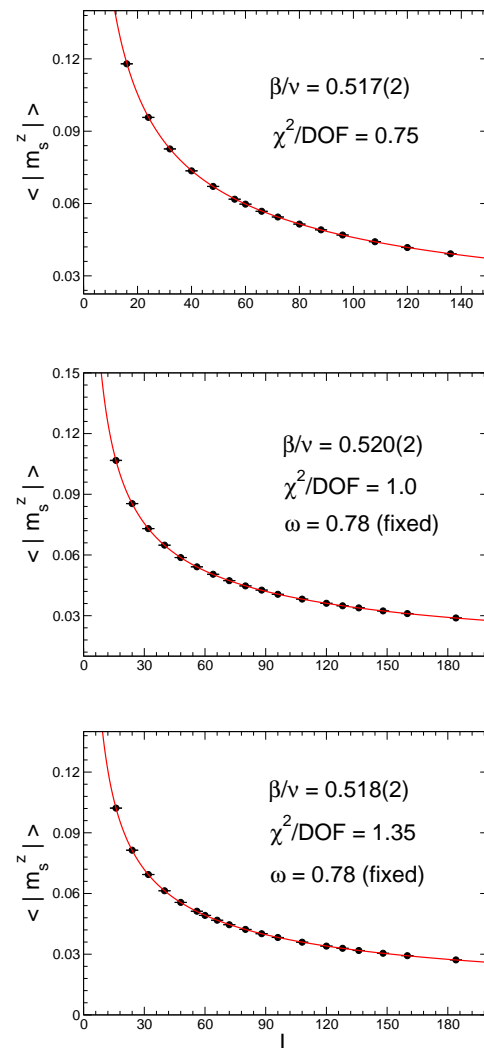


FIG. 6: Determination of  $\beta/\nu$  for the ladder- and herringbone-dimer models (top and middle panels) on the square lattice as well as for the staggered-dimer model on the honeycomb lattice (bottom panel). While  $\beta/\nu = 0.517(2)$  for the ladder-dimer model is obtained by fitting the 7 largest  $L$  data points of  $\langle |m_s^z| \rangle$  to their expected leading scaling behavior, fits with a fixed  $\omega = 0.78$  to  $\langle |m_s^z| \rangle$  of the herringbone-dimer model on the square lattice and the staggered-dimer model on the honeycomb lattice result in  $\beta/\nu = 0.520(2)$  and  $\beta/\nu = 0.518(2)$ , respectively.

as well as the staggered-dimer model on the honeycomb lattice. In particular, we determine the values of the exponents  $\nu$  and  $\beta/\nu$  with high accuracy by employing the finite-size scaling analysis to the relevant observables. Similar to the scenario found for the staggered-dimer model on the square lattice, while the observable  $\rho_{s1}2L$  of the staggered-dimer model on the honeycomb lattice receives a sizable correction to its scaling, the observable  $\rho_{s2}2L$  shows a good scaling behavior. As a result, using the data points of  $\rho_{s2}2L$  with moderate lattice sizes as well as the corresponding leading finite-size scaling



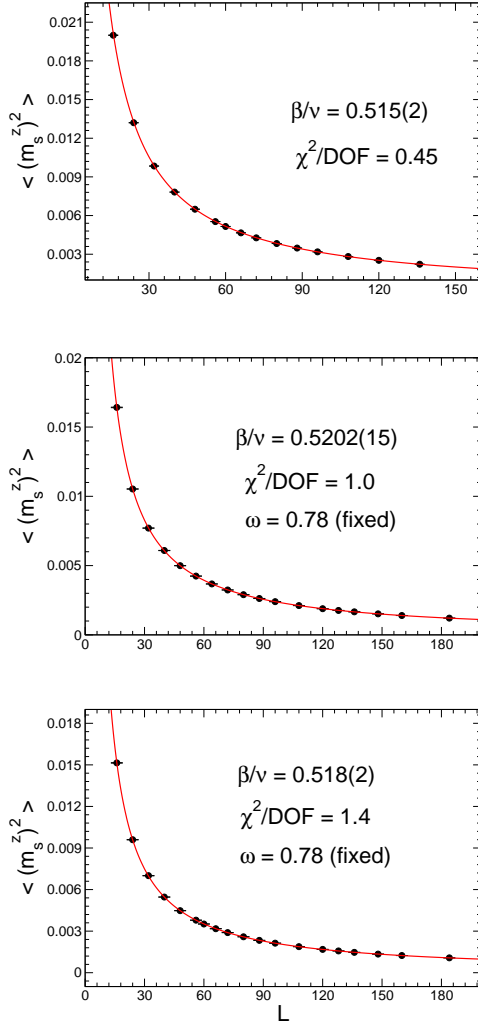


FIG. 7: Determination of  $\beta/\nu$  for the ladder- and herringbone-dimer models (top and middle panels) on the square lattice as well as for the staggered-dimer model on the honeycomb lattice (bottom panel). While  $\beta/\nu = 0.515(2)$  for the ladder-dimer model is obtained by fitting the 5 largest  $L$  data points of  $\langle (m_s^z)^2 \rangle$  to their expected leading scaling behavior, fits with a fixed  $\omega = 0.78$  to  $\langle (m_s^z)^2 \rangle$  of the herringbone-dimer model on the square lattice and the staggered-dimer model on the honeycomb lattice result in  $\beta/\nu = 0.5202(15)$  and  $\beta/\nu = 0.518(2)$ , respectively.

ansatz (letting  $b = 0$  in Eq. (5)), we are able to obtain a value for  $\nu$  consistent with the expected  $\nu = 0.7112(5)$  in the  $O(3)$  universality class. To understand this observation for the staggered-dimer model on both the square and honeycomb lattices from field theory aspect, is an interesting and important topic to explore. In particular, whether the cubic term introduced in [22] is responsible for this unexpected result should be investigated. Further, while it is argued in [22] that the herringbone-dimer model belongs to the category of models receiving a large correction, and our investigation supports this scenario, namely the values of  $\omega$  obtained from the fits related to

model	$L$	$\beta/\nu$	$\chi^2/\text{DOF}$
ladder	$72 \leq L \leq 136$	$0.517(2)^*$	0.75
ladder	$16 \leq L \leq 136$	$0.516(3)$	1.1
herringbone	$72 \leq L \leq 136$	$0.527(3)^*$	1.5
herringbone	$128 \leq L \leq 184$	$0.522(5)^*$	0.7
herringbone	$16 \leq L \leq 184$	$0.520(2)$	1.0
staggered	$72 \leq L \leq 136$	$0.531(3)^*$	1.2
staggered	$120 \leq L \leq 184$	$0.526(3)^*$	0.55
staggered	$16 \leq L \leq 184$	$0.518(2)$	1.35
ladder	$88 \leq L \leq 136$	$0.515(2)^*$	0.45
ladder	$16 \leq L \leq 136$	$0.515(2)$	1.3
herringbone	$128 \leq L \leq 184$	$0.525(4)^*$	1.25
herringbone	$16 \leq L \leq 184$	$0.5202(15)$	1.0
staggered	$128 \leq L \leq 184$	$0.527(4)^*$	1.1
staggered	$16 \leq L \leq 184$	$0.518(2)$	1.4

TABLE VI: The numerical values of  $\beta/\nu$  calculated from  $\langle |m_s^z| \rangle$  (the first 8 rows) and  $\langle (m_s^z)^2 \rangle$  (the last 6 rows) for the dimerized models considered in this study. All results are obtained with a fixed  $\omega = 0.78$  except those with a star which are determined by using the expected leading scaling prediction.

model	$\omega(\text{fixed})$	$\beta/\nu$	$\chi^2/\text{DOF}$
herringbone	1.0	$0.523(2)$	1.0
herringbone	0.9	$0.522(2)$	1.0
herringbone	0.7	$0.5181(23)$	1.06
herringbone	0.65	$0.5168(25)$	1.05
herringbone	0.6	$0.5152(27)$	1.04
herringbone	0.45	$0.5078(36)$	1.05
staggered	1.0	$0.523(2)$	1.55
staggered	0.9	$0.521(2)$	1.46
staggered	0.7	$0.5150(25)$	1.3
staggered	0.65	$0.5127(25)$	1.23
staggered	0.6	$0.5101(25)$	1.2
staggered	0.45	$0.4974(35)$	1.15

TABLE VII: The numerical values of  $\beta/\nu$  calculated from  $\langle |m_s^z| \rangle$  ( $16 \leq L \leq 184$ ) with variant fixed  $\omega$  for the fits.

$\rho_s L$  are all smaller than the expected  $\omega = 0.78$ , the same observable  $\rho_s L$  as well as  $Q_2$  are also compatible with the established result of  $\omega \sim 0.78$  in the  $O(3)$  universality class. Specifically, with a fixed  $\omega = 0.78$ , we are able to arrive at consistent  $\nu$  with  $\nu = 0.7112(5)$  from both  $\rho_s L$  and  $Q_2$  of the herringbone-dimer model. In order to clarify whether our data is really compatible with the scenario of an enhanced correction to scaling suggested in [22], it will be desirable to carry out a more detailed investigation to determine  $\omega$  with high precision. In particular, the consistence of the  $\nu$ , obtained from the fits using

model	$\omega(\text{fixed})$	$\beta/\nu$	$\chi^2/\text{DOF}$
herringbone	1.0	0.5232(12)	1.03
herringbone	0.9	0.5221(13)	1.0
herringbone	0.7	0.5185(15)	1.0
herringbone	0.65	0.5172(16)	1.0
herringbone	0.6	0.5156(18)	1.05
herringbone	0.45	0.5082(25)	1.1
staggered	1.0	0.5235(15)	1.7
staggered	0.9	0.5213(15)	1.55
staggered	0.7	0.515(2)	1.4
staggered	0.65	0.512(2)	1.35
staggered	0.6	0.509(2)	1.35
staggered	0.45	0.4920(36)	1.5

TABLE VIII: The numerical values of  $\beta/\nu$  calculated from  $\langle(m_s^z)^2\rangle$  ( $16 \leq L \leq 184$ ) with variant fixed  $\omega$  for the fits.

a fixed  $\omega = 0.78$ , with  $\nu = 0.7112(5)$  as shown in tables 2, 3, 4 and 5, is unlikely a coincidence considering the fact that the conclusion is valid for both the observables spin stiffness and second Binder ratio of both the herringbone- and ladder-dimer models. In addition, the finite-size scaling analysis performed for the determination of  $\beta/\nu$  suggests that, our data points for all the 2-d dimerized mod-

els with spatial anisotropy considered here are compatible with the established results of  $\beta/\nu = 0.519(1)$  and  $\omega \sim 0.78$  in the  $O(3)$  universality class as well. Finally, the consistence of the  $\beta/\nu$ , determined from the fits using a fixed  $\omega \in \{0.7, 0.9\}$ , with  $\beta/\nu = 0.519(1)$  implies that the observed enhanced correction to both the staggered- and herringbone-dimer models is because of the nonuniversal coefficients  $b_k$  in Eq. (6). Indeed, in tables 6, 7, and 8, the values of  $b_1$  and  $b_2$  determined from the fits associated with the herringbone- and staggered-dimer models are at least several times larger in magnitude than those of the ladder-dimer model. Whether there is a subtlety behind this observation or it is just a coincidence should be investigated since the determination of  $\omega$  might be contaminated by higher order terms. In conclusion, to explain what have been obtained in this study, a more detailed numerical study, and possibly a better theoretical understanding, for the critical theories of the models investigated here is required.

## VI. ACKNOWLEDGMENTS

Partial support from NSC (Grant No. NSC 99-2112-M003-015-MY3) and NCTS (North) of R.O.C. is acknowledged.

- 
- [1] M. Matsumoto, C. Yasuda, S. Todo, and H. Takayama, Phys. Rev. B **65**, 014407 (2001)
  - [2] M. Troyer, Prog. Theor. Phys. Supp. **145**, 326 (2002).
  - [3] L. Wang, K. S. D. Beach, and A. W. Sandvik, Phys. Rev. B **73**, 014431 (2006).
  - [4] C. Yasuda *et al.*, Phys. Rev. Lett. **94**, 217201 (2005).
  - [5] M. B. Hastings and C. Murdry, Phys. Rev. Lett. **96**, 027215 (2006).
  - [6] A. Praz, C. Murdy, and M. B. Hastings, Phys. Rev. B **74**, 184407 (2006).
  - [7] D. X. Yao and A. W. Sandvik, Phys. Rev. B **75**, 052411 (2007).
  - [8] K. H. Höglund, A.W. Sandvik, and S. Sachdev, Phys. Rev. Lett. **98**, 087203 (2007).
  - [9] K. H. Höglund and A.W. Sandvik, Phys. Rev. Lett. **99**, 027205 (2007)
  - [10] T. Pardini, R. R. P. Singh, A. Katanin and O. P. Sushkov, Phys. Rev. B **78**, 024439 (2008).
  - [11] F.-J. Jiang, F. Kämpfer, and M. Nyfeler, Phys. Rev. B **80**, 033104 (2009).
  - [12] S. Jin and A. W. Sandvik, arXiv:1110.5347.
  - [13] J. Oitmaa, Y. Kulik, and O. P. Sushkov, arXiv:1110.6478.
  - [14] S. Wenzel, L. Bogacz, and W. Janke, Phys. Rev. Lett. **101**, 127202 (2008).
  - [15] S. Chakravarty, B. I. Halperin, and D. R. Nelson, Phys. Rev. Lett. **60**, 1057 (1988).
  - [16] F. D. M. Haldane, Phys. Rev. Lett. **61**, 1029 (1988).
  - [17] A. V. Chubukov, S. Sachdev, and J. Ye, Phys. Rev. B **49**, 11919 (1994).
  - [18] S. Sachdev, *Quantum Phase Transitions* (Cambridge University Press, Cambridge, 1999).
  - [19] M. Vojta, Rep. Prog. Phys. **66**, 2069 (2003).
  - [20] M. Campostrini, M. Hasenbusch, A. Pelissetto, P. Rossi, and E. Vicari, Phys. Rev. B **65**, 144520 (2002).
  - [21] F.-J. Jiang, Rev. B **85** 014414 (2012).
  - [22] L. Fritz *et al.*, Phys. Rev. B **83**, 174416 (2011)
  - [23] M. Matsumoto, C. Yasuda, S. Todo, and H. Takayama, Phys. Rev. B **65**, 014407 (2001)
  - [24] A. F. Albuquerque, M. Troyer, and J. Oitmaa, Phys. Rev. B **78**, 132402 (2008).
  - [25] S. Wenzel and W. Janke, Phys. Rev. B **79**, 014410 (2009).
  - [26] F.-J. Jiang and U. Gerber, J. Stat. Mech. P09016 (2009).
  - [27] S. Wenzel, PhD thesis, Universität Leipzig (2009).
  - [28] H. G. Evertz, G. Lana, and M. Marcu, Phys. Rev. Lett. **70**, 875 (1993).
  - [29] H. G. Evertz, Adv. Phys. **52**, 1 (2003).
  - [30] U.-J. Wiese and H.-P. Ying, Z. Phys. B **93**, 147 (1994).
  - [31] B. B. Beard and U.-J. Wiese, Phys. Rev. Lett. **77** (1996) 5130.
  - [32] A. F. Albuquerque *et al.*, Journal of Magnetism and Magnetic Material **310**, 1187 (2007).
  - [33] M. E. Fisher and M. N. Barber, Phys. Rev. Lett. **28**, 1516 (1972).
  - [34] E. Brézin, J. Phys. (Paris) **43**, 15 (1982).
  - [35] M. N. Barber, in *Phase Transitions and Critical Phenomena*, ed. C. Domb (Academic, New York, 1983), Vol. 8.
  - [36] E. Brézin and J. Zinn-Justin, Nucl. Phys. B **257**, 867

- (1985).
- [37] M. P. A. Fisher, P. B. Weichman, G. Grinstein, and D. S. Fisher, Phys. Rev. B **40**, 546 (1989).